Intermetallics 131 (2021) 107110

Contents lists available at ScienceDirect

Intermetallics

journal homepage: http://www.elsevier.com/locate/intermet

Crystal structure and phase composition evolution during heat treatment of Fe-45Ga alloy

T.N. Vershinina [a,*], I.A. Bobrikov [a,b], S.V. Sumnikov [a,b], A.O. Boev [c], A.M. Balagurov [a,b,d], A. K. Mohamed [b], I.S. Golovin [b]

[a] Joint Institute Or Nuclear Research, Dubna, Russian Federation
[b] National University of Science and Technology "MISIS", Moscow, Russian Federation
[c] Skolkovo Institute of Science and Technology, Bolshoy Boulevard, Bld. 1, Moscow, 121205, Russian Federation
[d] Lomonosov Moscow State University, Moscow, Russian Federation

ARTICLE INFO

Keywords:
Fe–Ga alloys
Atomic structure
Phase transformation
Neutron diffraction
X-ray diffraction
DFT

ABSTRACT

The atomic structure of the high-temperature β-Fe_6Ga_5 phase, formed in the Fe-45at.%Ga alloy during rapid cooling from the melt, has been refined by X-ray, neutron diffraction techniques, and density functional theory calculations. The regularities of the phase composition evolution of the quenched Fe-45at.%Ga alloy in the process of continuous slow heating and cooling under vacuum conditions have been revealed. It is shown that after the heating-cooling cycle, the structures of the outer layers and the sample volume are completely different.

1. Introduction

Structural types and features of the iron-gallium phase diagram have been the subject of interest in numerous studies since the 1960s. The results obtained before the 1990s are adequately represented in the H. Okamoto review [1], which contains a diagram of stable phases of Fe-*x*Ga in the entire range of gallium concentrations ($0 \leq x \leq 100\%$) and the crystallographic data (space group and unit cell parameters) for the main stable and some metastable compositions. In the early 2000s, the interest in the structure of Fe–Ga alloys became high again after the discovery of increased magnetostriction values for the gallium content $x \approx$ (17–19) and (26–27) at.% [2,3], which is now referred to as "giant magnetostriction" [4]. This discovery led to the appearance of many papers in which the features of the structural transformations and phase transitions between different structural states of Fe–Ga alloys in this concentration range were studied. At present, it can be assumed that up to $x \approx 30$ at.% the situation is generally clear [5]. Namely, the equilibrium states of the Fe–Ga system include phases with a disordered atomic structure (A1, A2, and A3) and phases with a partially ordered structure (B2, $D0_3$, $D0_{19}$, and $L1_2$). The ranges for the existing single A2 and $L1_2$ phases have been recently refined in Refs. [6,7]. The description of all the phases and their structural data, including the positions of atoms in the unit cell, can be found in the reference book [8–10].

In the review [1] for $x > 30$ at.%, the compositions of the α-Fe_6Ga_5, β-Fe_6Ga_5, Fe_3Ga_4, $FeGa_3$ are indicated as the equilibrium phases and $Fe_{13}Ga_9$ as a metastable one. According to the phase diagram, the β-Fe_6Ga_5 phase is a high-temperature (temperature range $T \approx$ 770-800 °C) state, which at lower temperatures should transform into the α-Fe_6Ga_5 state. The crystallographic data of α-Fe_6Ga_5 (Fe-45.5Ga) are $a = 10.058$ Å, $b = 7.946$ Å, $c = 7.747$ Å, $\beta = 109.33°$, $Z = 4$, $V_a = 13.39$ Å^3, sp. gr. *C*2/*m* (№12) as it was presented in Ref. [11] together with the atomic coordinates. The situation with the β-Fe_6Ga_5 phase is less clear. H. Okamoto provides only the crystallographic data for the Fe-45Ga phase (rhombohedral setting): *R*3*m* (No.160), $a_R = 8.841$ Å, $\alpha_R = 89.2°$, with reference to Ref. [12]. At the same time, in Ref. [13], for the composition Fe_7Ga_6 (Fe-46.2Ga), almost identical cell parameters are given: $a_R = 8.81$ Å, $\alpha_R = 89.2°$, which for the hexagonal setting correspond to $a_H = 12.372$ Å, $c_H = 15.471$ Å. Finally, in a relatively recent paper [14], the structure of the $Fe_{13}Ga_{13}$ phase (Fe-50Ga, denoted as ζ_2-GaFe) was determined: sp. gr. *R*-3*m* (№166), $a_H = 12.437$ Å, $c_H = 7.764$ Å. It means that the space group is centrosymmetric and the lattice is the same as for Fe_7Ga_6 in Refs. [12,13], though c_H is two times shorter.

Previously we conducted a systematic study of the structure and phase transitions in Fe-xGa alloys with a concentration range of gallium

* Corresponding author.
E-mail addresses: vershinina@nf.jinr.ru (T.N. Vershinina), bobrikov@nf.jinr.ru (I.A. Bobrikov), sumnikovsv@gmail.com (S.V. Sumnikov), A.Boev@skoltech.ru (A.O. Boev), bala@nf.jinr.ru (A.M. Balagurov), abdelkarim.abdelkarim@feng.bu.edu.eg (A.K. Mohamed), i.golovin@misis.ru (I.S. Golovin).

https://doi.org/10.1016/j.intermet.2021.107110
Received 26 November 2020; Received in revised form 14 January 2021; Accepted 15 January 2021
Available online 27 January 2021

$9 \leq x \leq 38\%$ [15,16]. As a continuation of this study, the X-ray and neutron diffraction patterns of the as-cast Fe-45Ga alloy were measured. Almost all the observed diffraction peaks were successfully indexed within the unit cell proposed in Ref. [14]. This means that for the Fe-45Ga as-cast sample instead of the assumed equilibrium α-Fe_6Ga_5 phase, the nonequilibrium high-temperature state β-Fe_6Ga_5 was retained during casting.

In the present study, the atomic structure of the Fe-45Ga alloy was refined using X-ray (XRD) and neutron diffraction (ND) techniques, as well as density functional theory (DFT) calculations. As an initial approximation, we use the data obtained in Ref. [14] for the Fe-50Ga ($Fe_{13}Ga_{13}$) alloy. In addition, the structural transformations of the Fe-45Ga composition in various layers of the samples during slow heating and subsequent cooling were studied. It is shown that the heating-cooling cycle leads to radically different structures of the surface layers and volume of the sample.

2. Materials and methods

The Fe–Ga alloy with the nominal composition 45 at.% Ga was produced in an Indutherm MC-20 V mini furnace by induction melting under protective high-purity argon gas and cast out in the copper mold (4x16 × 60 mm) with an average cooling rate of 2000 K/min. The alloy disintegrated into small part during casting at the ingot solidification stage. The chemical composition analysis by EDX Spectroscopy revealed that the sample composition in a volume is indeed Fe-45.0 ± 0.1 at.% Ga though in the upper layer of the sample, it is Fe-44.1 ± 0.3 at.% Ga (in this paper, we use only atomic %). According to Kubashewski [17] and Okamoto [1] Fe–Ga phase diagrams, both compositions belong to a single-phase range. To study the alloy structure, we used this as-cast sample.

The XRD structural analysis was performed at room temperature using an EMPYREAN (PANalytical) powder diffractometer with the Cu-K_α radiation. The study of the phase composition evolution during heating to 770 °C and subsequent cooling was carried out using an AntonPaar HTK 1200 N high-temperature attachment. The *in situ* experiment was carried out with heating and cooling rates of 2°C/min. The data acquisition time for one diffraction pattern in the angular range 2θ = 10-85° was 2 min, the total time of the experiment was ~15 h. Before the XRD studies, the sample surface was mechanically ground and polished.

The neutron diffraction patterns were measured with a high-resolution ($\Delta d/d \approx 0.0015$) Fourier diffractometer (HRFD) operating at the IBR-2 pulsed reactor in JINR (Dubna, Russia) [18]. In the high-resolution mode, the diffraction spectrum was measured up to d_{hkl} = 4 Å. The measurements of higher d_{hkl} and *in situ* study were performed in the medium resolution ($\Delta d/d \approx 0.015$) mode. The sample was examined without preliminary removal of the surface layer.

Calculations of the full energies and optimized geometries were performed in the framework of the DFT [19] using Vienna *ab initio* simulation package (VASP) [20] and high-throughput python-based package SIMAN [21]. The exchange-correlation energy was evaluated by a generalized gradient approximation (GGA) within the Perdew-Burke-Ernzerhof (PBE) functional [22]. The kinetic energy cutoff of 350 eV, the k-spacing parameter of 0.2 $Å^{-1}$, and the Fermi-level smearing width of 0.2 eV were chosen. Iron and gallium PAW-pseudopotentials with $3d^74s^1$ and $4s^24p^1$ valence electrons, respectively, were used for DFT calculations. The initial magnetic moments were set as 5.0 and 0.6 μB for Fe and Ga, respectively. The conjugate-gradient method and the relaxation of atomic positions and supercell volume (maximum force acting on atoms less than 25 meV/Å) were used to obtain optimized geometry. The values of the formation energy were obtained by the equation $E_f = E(N) - \Sigma_i \mu_i n_i$, where $E(N)$ is the energy of supercell consisting of N atoms, μ is the chemical potential of the i-element, and n is the number of the i-element in the supercell. The chemical potentials of Fe and Ga were taken from the Materials Project DFT database [23].

The Rietveld refinement of the cell parameters and the atomic positions was conducted using the Powder Cell 2.4 program [24] for the X-ray data and the FullProf software package [25] for neutron data. The occupancy factors for the Fe and Ga sites were fixed to 1.

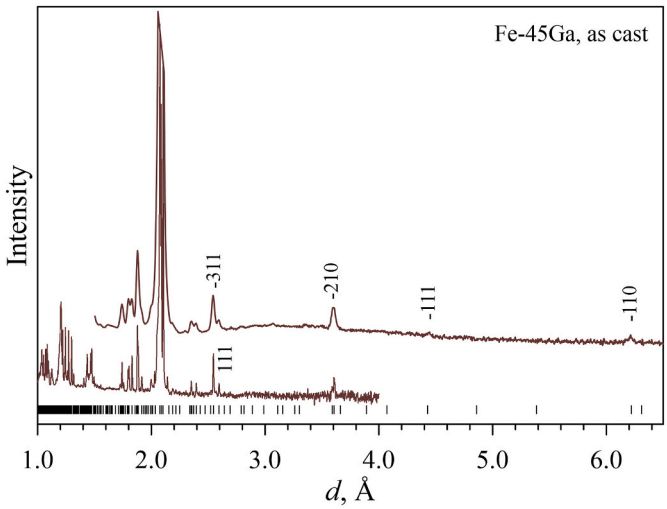

Fig. 1. Neutron diffraction patterns of the as-cast sample measured in high- (lower curve) and medium- (upper curve) resolution modes. The intensity scales are offset relative to each other. At $d_{hkl} > 6.5$ Å there are no intensive diffraction lines. The calculated positions of diffraction peaks for the $Fe_{13}Ga_{13}$ phase are shown.

3. Results

3.1. Atomic structure of $Fe_{13}Ga_{13}$

In Fig. 1, the neutron diffraction patterns of the *as-cast* sample measured with HRFD in both resolution modes are shown. One can see that the positions for practically all diffraction lines can be described in the frame of the rhombohedral unit cell with the constants $a_R = 7.637$ Å, $\alpha_R = 109.07°$, which are equivalent to hexagonal setting with a_H = 12.440 Å, $c_H = 7.785$ Å. These values coincide well (better than 0.3% accuracy) with the data from Ref. [14]. It means that the atomic structures of Fe_7Ga_6 (Fe-46.2Ga) [13] and $Fe_{13}Ga_{13}$ (Fe-50Ga, ζ_2-GaFe) [14] are the same and correspond to the β-Fe_6Ga_5 phase (Fe-45.5Ga), appearing in the phase diagrams in the Okamoto review [1]. For definiteness, below, we designate this phase as $Fe_{13}Ga_{13}$ and assume that it corresponds to our composition of Fe-45Ga.

The neutron diffraction pattern of the as-cast samples exhibits reflections not only from the $Fe_{13}Ga_{13}$ phase. The bcc-derivative structure (A2, B2, or $D0_3$) in a small amount (~5%) can be noted. It was not reliably interpreted since its possible superstructure reflections from B2 or $D0_3$ cannot be properly distinguished. Accordingly, it can be either disordered A2 or partially ordered derivatives of the A2 phase (B2 or $D0_3$ phases). But according to the Fe–Ga phase diagram [1], a region of equilibrium B2 phase is above the region of existence of the β-Fe_6Ga_5 phase. Thus, it can be assumed that just the B2 phase is present in the quenched alloy. In addition, this assumption matches the revealed in Ref. [13] tendency of the B2 phase to form with increasing the Ga content in Fe–Ga alloys. The diffraction pattern also shows low-intensity peaks, which can be caused by an insignificant amount of the α-Fe_6Ga_5 and Fe_3Ga_4 phases. The Rietveld refinement of the neutron diffraction pattern confirmed that $Fe_{13}Ga_{13}$ is the main phase (>90%) in this sample.

The phase analysis performed using the XRD showed that the as-cast sample contains $Fe_{13}Ga_{13}$ (~95%) and the B2 phase, while the α-Fe_6Ga_5 and Fe_3Ga_4 phases are not determined in contrast to the neutron data. In

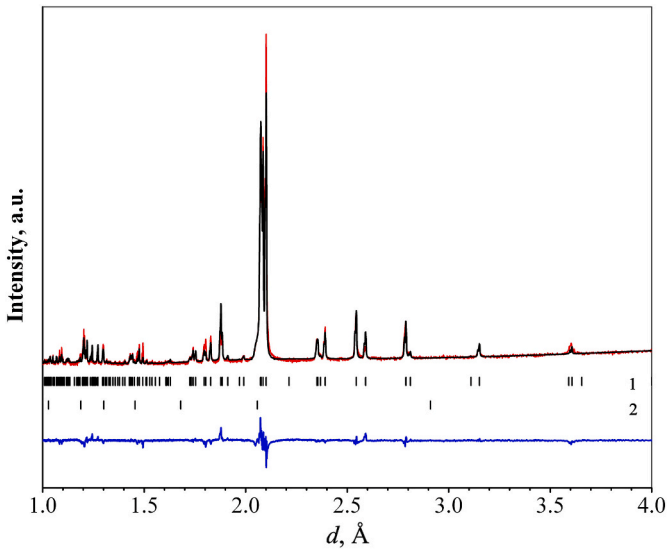

Fig. 2. Measured (red line) and calculated (black line) XRD patterns of the *as-cast* Fe-45Ga alloy. The Rietveld refinement was carried out using the coordinates obtained by the DFT method. The difference function and the positions of the diffraction peaks for the $Fe_{13}Ga_{13}$ and B2 phases (upper and lower rows, respectively) are shown.

Table 1
Structural data and refinement conditions for $Fe_{13}Ga_{13}$.

	XRD	ND
Sample size	10 mm × 8 mm × 4 mm	
Analyzed volume	upper layer of polished sample with thickness ~2 μm	whole sample
Formula weight	1632.38 g/mol	
Crystal system	hexagonal	
Space group	R-3m	
Lattice constants, hexagonal setting	a = 12.442 ± 0.002 Å, c = 7.773 ± 0.002 Å	a = 12.4433 ± 0.0003 Å, c = 7.7887 ± 0.0002 Å
Atomic volume, V_a	13.360 Å^3	13.390 Å^3
Formula units	3	3
Radiation	Cu-Kα	white beam (TOF)
Temperature	25 °C	
d, Å	1.13–8.84	0.96–4.2
Diffractometer	EMPYREAN (PANalytical)	HRFD
Rotation	0° ≤ ω ≤ 360°	without rotation
Refinement	PowderCell 2.4 (SOF = 1 and B_{iso} = 0.5)	FullProf (SOF = 1 and B_{iso} = 0.5)
χ^2, R_{wp}	8.76, 1.32%	3.10, 5.56%

this regard, it should be noted that before the XRD experiment, the surface was ground and polished, i.e., the top layer was removed, and the interior of the sample was examined. In the case of ND, the sample was investigated in its initial state, and both its internal and external parts fell into the analysis area. It is known that the differences in the cooling rate of the surface layer and the internal volume can lead to the formation of different phase compositions in them (see, for example [15]). Thus, it is obvious that the phase composition differences are associated with the difference in the analyzed volumes. It is most likely that, in our case, the α-Fe_6Ga_5 and Fe_3Ga_4 phases are precipitated in the surface layer of the quenched sample.

The comparison of our experimental XRD spectrum with the spectrum simulated using the coordinates from Ref. [14] showed several inconsistencies. There are some discrepancies in the intensity of the peaks and the presence of the peaks in the simulated spectrum that were not observed experimentally. The factors that characterize the experimental and simulated spectra's correspondence are as follows: χ^2 = 12.33, R_{wp} = 1.58%. The structure optimization with refining of atomic positions given in Ref. [14] was made using DFT. The data for Mn and Ga were taken as the initial values of the atomic coordinates from Ref. [26], but manganese atoms were replaced by iron atoms. The refinement of the coordinates of iron and gallium atoms made it possible to significantly reduce the discrepancy between the experimental and simulated XRD spectra (χ^2 = 8.76, R_{wp} = 1.32%) (Fig. 2). The presence of the B2 phase was taken into account during processing of the experimental XRD patterns. The refinement conditions and structural data are given in Table 1 and Table 2. The data obtained by the Rietveld method are in good agreement with the DFT results. Thus, the mean absolute error (MAE) for the distances between the nearest neighbors Fe–Fe, Fe–Ga, and Ga–Ga does not exceed 0.02 Å, and the difference between the atomic volumes V_a, does not exceed 1%. This is an excellent result for the DFT analysis [27,28].

The agreement between the experimental data obtained by the ND method and the simulated pattern is also good. The conventional weighted R_{wp}-factor and χ^2-value are 5.56% and 3.10, correspondingly. The refined neutron coordinates are also given in Table 2.

Table 3 summarizes formation energy of the $Fe_{13}Ga_{13}$ phase with different atomic configurations calculated by DFT. As can be seen, the most stable crystal structure is characterized by an equal number of gallium and iron atoms. The replacement of gallium atoms by iron atoms, as well as a decrease in the degree of the occupancy of the equivalent positions of gallium atoms (introduction of vacancies) leads to an increase in the formation energy of the high-temperature phase $Fe_{13}Ga_{13}$. Calculations show that the most preferred sites for the replacement of gallium atoms by iron atoms are the sites corresponding to the Wyckoff position 18h.

Thus, the designation $Fe_{39}Ga_{39}$ used in Ref. [14] is the most correct. The presence of the phase with a predominance of iron (which also includes the B2 phase) in addition to the $Fe_{13}Ga_{13}$ phase is quite natural for the quenched Fe-45Ga alloy.

3.2. Phase evolution during heating and cooling

Notably, the investigated structure corresponds to the pronounced nonequilibrium state of the Fe-45Ga alloy that was produced immediately after casting from the melt into a copper mold. Upon annealing or continuous heating, this structure will decompose with the formation of equilibrium phases. Fig. 3 shows the evolution of the XRD spectra measured during continuous heating of the Fe-45Ga alloy in the as-cast state from room temperature to 770 °C, holding at this temperature for 90 min and subsequent cooling at a rate of 2 °C/min. The individual diffraction patterns were measured with 2 min exposure time and processed by the Rietveld method to obtain the phase content. As follows from the analysis of the phase composition (Fig. 4a), $Fe_{13}Ga_{13}$ and a small amount of B2 are present at the initial heating stages. This pattern is observed up to 450 °C and is accompanied by a regular increase in the crystal lattice parameters of the $Fe_{13}Ga_{13}$ phase (Fig. 5). The variation of the lattice parameter with temperature is described by second-order polynomials. The fitting by the least squares method gives the following equations:

$$a(T) = 12.4414 + 0.8 \times 10^{-4}T + 2.5 \times 10^{-7}T^2, c(T) = 7.7773 + 1.3 \times 10^{-4}T + 8.9 \times 10^{-8}T^2$$

A gradual decrease in the volume fraction of $Fe_{13}Ga_{13}$ occurs at temperatures above 450 °C, and at $T \approx 610$ °C it completely disappears. Also, at 450 °C, the diffraction patterns show the appearance of peaks belonging to the fcc based lattice, which is designated as A1 in the figures. The volume fraction of the A1 phase reaches a maximum of ~43% at 590 °C, then sharply decreases to a level of ~5% at 610 °C, and disappears at 725 °C. The A3 phase has the hcp lattice (there are no superstructural peaks from $D0_{19}$ on the XRD patterns), and it is present in the alloy in a temperature range of 600–700 °C at instant heating. The

Table 2
Refined fractional atomic coordinates (x, y, z) for $Fe_{13}Ga_{13}$: the DFT calculations (first rows), the Rietveld refinement of the XRD pattern (second rows) and the Rietveld refinement of the ND pattern (third rows). The space group: R-3m (№ 166), the lattice parameters and the atomic volume calculated by DFT are: $a = 12.485 \pm 0.001$ Å, $c = 7.718 \pm 0.001$ Å, $V_a = 13.3589$ Å^3.

No	Site notation	Atom	Multiplicity	Wyckoff position	x	y	z
1	Ga1	Ga	3	a	0	0	0
2	Ga2	Ga	18	h	0.1018	0.5509	0.0910
					0.1013 (3)	0.5507 (2)	0.0909 (6)
					0.0988 (2)	0.5494 (1)	0.0891 (3)
3	Ga3	Ga	18	g	0	0.3882	0.5
					0	0.3854 (3)	0.5
					0	0.3834 (5)	0.5
4	Fe1	Fe	3	b	0	0	0.5
5	Fe2	Fe	18	h	0.2326	0.1163	0.9168
					0.2345 (2)	0.1173 (2)	0.9223 (4)
					0.2368 (1)	0.1184 (1)	0.9275 (2)
6	Fe3	Fe	18	h	0.8539	0.9270	0.7504
					0.8555 (3)	0.9277 (3)	0.7502 (5)
					0.8532 (1)	0.9266 (1)	0.7508 (3)

Table 3
DFT calculated formation energies (in eV) of Ga_xFe_y supercells with different x and y.

Configuration	Description	Formation energy, eV
$Ga_{39}Fe_{39}$	Without substitution	−2.38
$Ga_{38}Fe_{40}$	Substitution of one atom	from −1.91 to −1.25
$Ga_{37}Fe_{41}$	Substitution of two atoms	from −1.43 to 0.16
$Ga_{36}Fe_{42}$	Substitution of three atoms	from −0.94 to 0.16
$Ga_{38}Fe_{39}$	Vacancy introduction	from −0.79 to −0.19

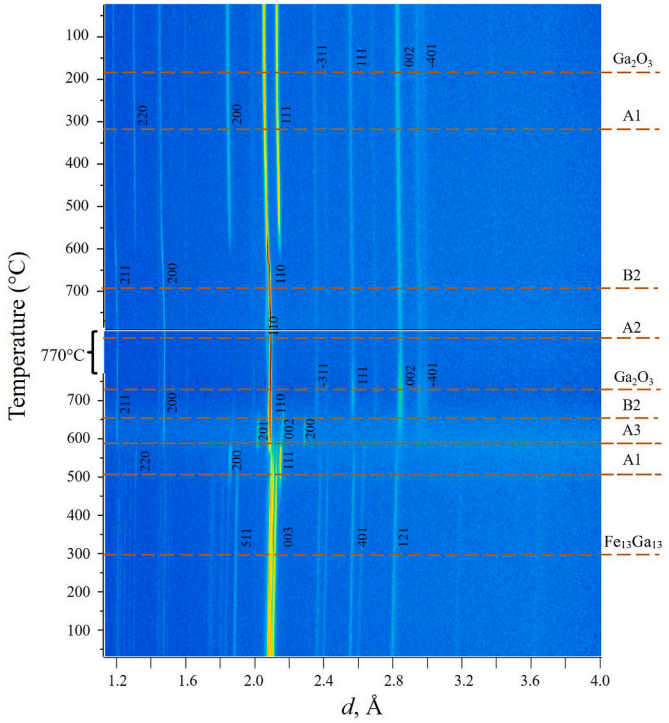

Fig. 3. 2D visualization of the XRD diffraction pattern evolution of the Fe-45Ga sample in the as-cast state measured upon slow heating up to 770°C, annealing at this temperature for 90 min, and subsequent cooling down in the real-time mode. The temperature (and time) axis goes from bottom to top; the d-spacing axis goes from left to right. Both heating and cooling were performed with a rate of 2 °C/min.

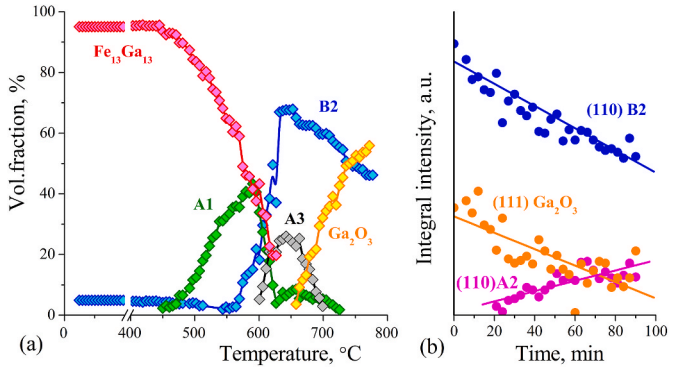

Fig. 4. Evolution of the phase composition in the surface layer of the Fe-45Ga alloy upon heating to 770 °C (a) and the integrated intensities of individual peaks of the B2, A2, and Ga_2O_3 phases during subsequent isothermal holding for 90 min (b) (XRD).

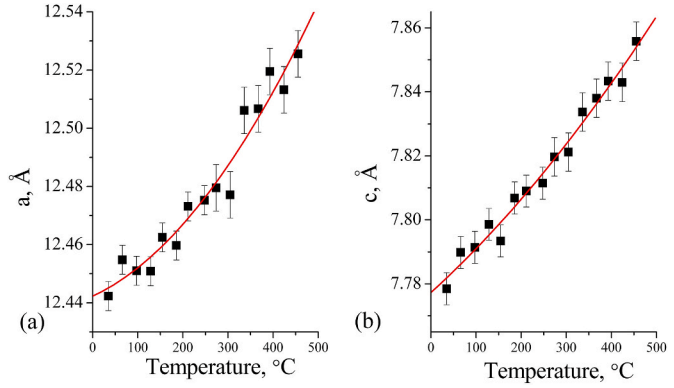

Fig. 5. Lattice parameters of the $Fe_{13}Ga_{13}$ phase as a function of temperature.

volume fraction of the bcc-originated phase, which was initially present in the alloy in an amount of ~5%, begins to increase at 570 °C and reaches its maximum at ~640 °C. At this temperature, this phase can be interpreted as B2 on the base of the appearance of a superstructure reflection. However, because at $T \approx 610$ °C a gallium oxide layer (β-Ga_2O_3, monoclinic, C2/m) begins to form on the sample surface, the volume fraction of the B2 phase in the analyzed layer gradually decreases. It does not exclude the preservation of the bcc phase fraction in bulk under the oxide. The fraction of the β-Ga_2O_3 oxide, in which, according to the literature [29], the dissolution of an insignificant amount

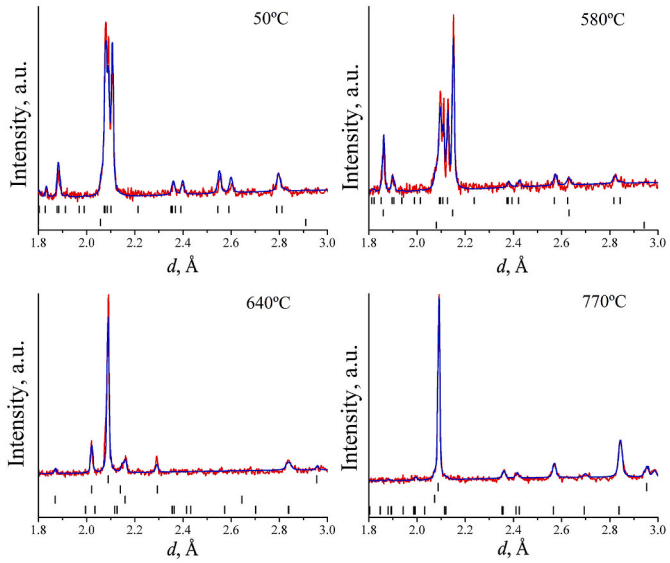

Fig. 6. XRD diffraction patterns measured upon heating for several characteristic temperatures and processed by the Rietveld method. The experimental points and the calculated line are shown. The vertical bars indicate the peak positions of the presented phases (from top to bottom): $Fe_{13}Ga_{13}$, B2 (50 °C); $Fe_{13}Ga_{13}$, $L1_2$, B2 (580 °C); B2, A3, $L1_2$, Ga_2O_3 (640 °C); B2, A2, Ga_2O_3 (770 °C).

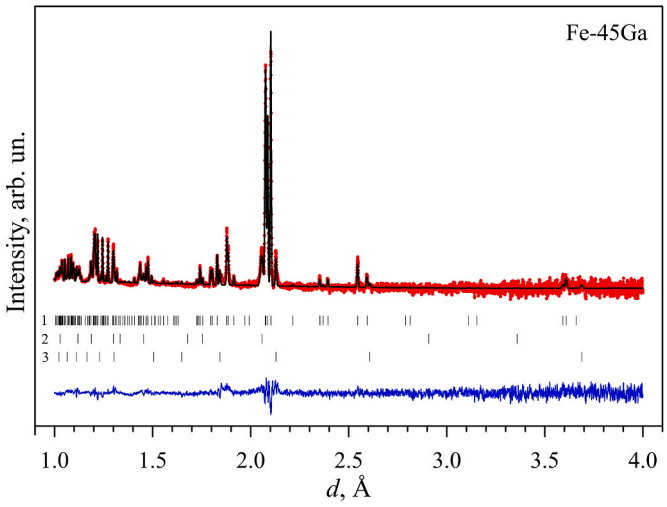

Fig. 7. Rietveld refinement pattern of the as-cast Fe-45Ga sample measured at the HRFD at room temperature after the heating-cooling process. The experimental points, the calculated profile, and the difference plot (in the bottom) are shown. The difference is weighted by the mean-squares deviation for each point. The vertical bars indicate the peak positions (from top to bottom) of: $Fe_{13}Ga_{13}$ (1), B2 (2), $L1_2$ (3). At $d_{hkl} > 4.0$ Å there are no intensive diffraction lines.

of iron is possible, rather rapidly grows with increasing temperature. The examples of the Rietveld refinements for some particular phase states are shown in Fig. 6.

Thus, according to the XRD data, the phase evolution observed during heating, as we suppose, can be represented as a scheme: $Fe_{13}Ga_{13} + B2 \rightarrow B2 + L1_2 \rightarrow B2 + D0_{19} \rightarrow B2 + A2 + Ga_2O_3$. The most remarkable thing is that, contrary to our expectations, the $Fe_{13}Ga_{13}$ phase was not transformed into the α-Fe_6Ga_5 phase but disappeared. In general, the presented scheme of transitions corresponds to the scheme observed in Fe-(25–27) Ga alloys, namely, $D0_3 \rightarrow L1_2 \rightarrow D0_{19} \rightarrow A2$ (see, for example [30]).

The gallium content in the layer directly below the oxide was estimated for the state at 770 °C on the base of the volume fraction of the phases presented in the analyzed volume. It was found that the total gallium concentration at this layer continuously decreases from 45 to ~21 at.%. Most likely, a gallium gradient is formed in the direction from the volume to the surface. A similar situation was observed in Ref. [31] for the Fe–27Ga alloy. The elemental analysis of the surface layer conducted after the *in situ* XRD experiment with heating up to 850 °C reveals a deficiency of gallium on its outer surface. The refined elemental composition was found to be close to Fe–16Ga.

Estimation of the thickness of the surface layer analyzed by XRD showed a value of $t \approx 3$ μm for the Fe-45Ga composition. Since the coefficient of mass attenuation of Cu-Kα radiation for iron is five times greater than for gallium [32], then as gallium leaves the alloy, the thickness of the analyzed layer will naturally decrease to ~1.8 μm for pure iron.

During isothermal holding at 770 °C (Fig. 4b), the integral intensities of the characteristic for the β-Ga_2O_3 peaks decrease. Apparently, this is due to the fact that gallium diffuses from the bulk to the surface, and in the presence of the residual oxygen, the Ga_2O_3 oxide forms. Upon further release of gallium from the alloy, a reaction $Ga_2O_3(s) + 4Ga(l) \rightarrow 3Ga_2O(g)\uparrow$ occurs [33]. As a result, a volatile compound Ga_2O is formed, and the amount of oxide Ga_2O_3 on the surface decreases.

The analysis of the integral intensities of the characteristic peaks of the bcc phase B2 showed (Fig. 4b) that they decrease monotonically. The most probable reason for this is the formation of one more phase based on the bcc lattice (apparently, A2) with a cell parameter lower than that of B2 during the exposure. A new phase appears after 20 min of exposure at 770 °C. The intensity of its diffraction peaks increases linearly, and the cell parameter gradually decreases, i.e., the difference with the cell parameter of the B2 phase increases. These trends, which include a decrease in the intensities of the Ga_2O_3 and B2 peaks, an increase in the A2 content, and a decrease in the parameter of its cell, indicate the complex nature of the processes taking place. In particular, the change in the cell parameter of the A2 phase can be associated with a decrease in the gallium concentration in it (see, for example [15,34]).

It should be noted that a decrease in the intensities of the diffraction peaks of the bcc phase at high temperatures, which is not associated with the formation of new phases, has already been observed for some compositions of Fe-Ga [35] and Fe–Al [36] alloys in neutron experiments. No reliable explanation was found for this effect: in the opinion of the authors of these studies, it was associated with a variation of the extinction coefficient with a change in the degree of structural imperfection.

Based on the obtained results, it can be assumed that the alloy composition of the material in the volume analyzed by the XRD method shifts to the concentration of gallium <45 at% during temperature manipulations. There are data in the literature indicating that when Fe–Ga alloys are heated in vacuum, gallium evaporates from the layers adjacent to the surface. Thus for the alloy ($Fe_{81.3}Ga_{18.7}$ + 0.5 at.%B + 0.005 at.%S), it was found that after annealing at 1100 and 1200 °C in the plates with a thickness of 0.30–0.35 mm the gallium concentration decreases to values of 0–0.2 at.% [37].

During cooling (Fig. 3), the elemental composition of the surface layer homogenized, and the A2 phase vanished already at ~620 °C. In the same temperature range (~600 °C), the formation of the A1 phase begins. It exists up to room temperature together with B2 and Ga_2O_3. Thus, by the XRD technique neither the high-temperature $Fe_{13}Ga_{13}$ nor the low-temperature α-Fe_6Ga_5 phases after the heating-cooling cycle are detected.

Fig. 7 shows the result of processing by the Rietveld method of the neutron diffraction pattern of the same bulk sample after its heating to 770°C and subsequent cooling with a rate of 2°C/min. As well as before heating, the main phase is $Fe_{13}Ga_{13}$ in the amount of 85%. In addition, the phases B2 (6%) and $L1_2$ (9%) are recorded. The gallium oxide β-Ga_2O_3 is not detected by neutron diffraction due to its small volume

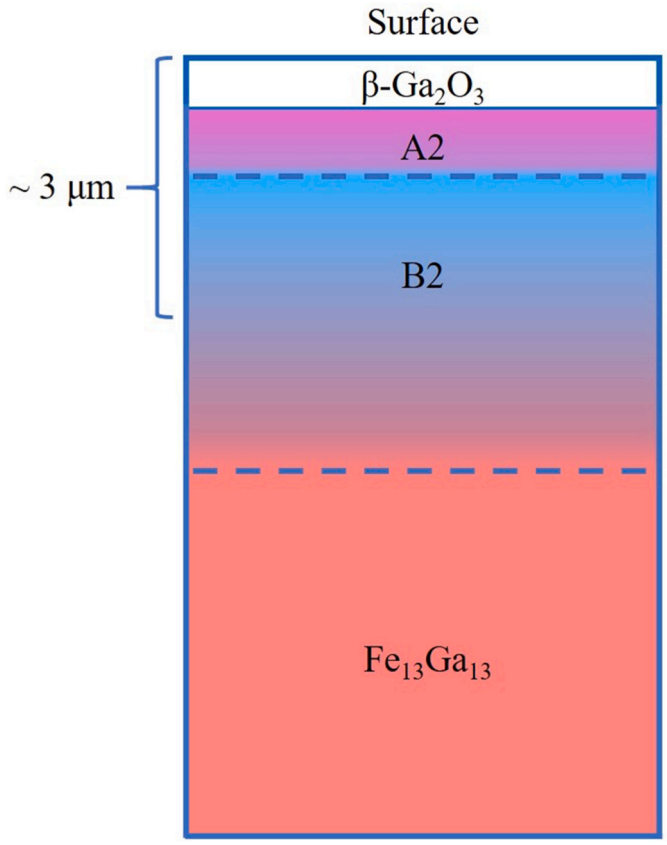

Fig. 8. Schematic representation of the surface layer of the alloy Fe–45.0%Ga after heating up to 770 °C.

fraction. As in the case of the as-cast state, the phase composition determined from the neutron data differs from the X-ray one. The obvious reason is the difference in the compositions on the surface and in the bulk of the sample.

It can be argued that heating and holding at 770 °C is not enough for the $Fe_{13}Ga_{13} \rightarrow \alpha\text{-}Fe_6Ga_5$ transformation, which was expected according to the Fe–Ga phase diagram [1]. In the case of annealing in vacuum, a structure shown schematically in Fig. 8, was formed due to the formation of a gallium distribution gradient in the direction from the bulk to the surface.

4. Conclusions

This work presents the structural analysis of the quenched Fe-45Ga alloy by X-ray and neutron diffraction techniques and numerical simulation. As a result of rapid cooling of the ingot, the high-temperature $Fe_{13}Ga_{13}$ phase is preserved in the sample. Contrary to the data given by Okamoto [1], the unit cell parameters of this phase are close to the parameters that were determined for the Fe-50Ga composition in Ref. [14]: sp. gr. *R*-3*m* (№166), $a_H = 12.437$ Å, $c_H = 7.764$ Å. The atomic coordinates were refined by first principles calculation and the Rietveld processing of the XRD and ND patterns. All values obtained are close to each other and only slightly differ from the atomic coordinates given in Ref. [14] for Fe-50Ga (ζ_2-GaFe). Thus, we conclude that the atomic structures reported in several papers as Fe_7Ga_6 (Fe-46.2Ga) [13], $Fe_{13}Ga_{13}$ (Fe-50Ga, denoted as ζ_2-GaFe) [14], and $\beta\text{-}Fe_6Ga_5$ (Fe-45.5Ga) studied in this paper and indicated earlier in the phase diagram [1] are the same. The results obtained in this work indicate that the most correct designation is $Fe_{13}Ga_{13}$.

By *in situ* XRD, it is found that under heating up to 770 °C, gallium evaporates from the surface of the Fe-45Ga alloy. This leads to a change in the phase composition and influences on the recorded temperatures of phase transitions in the alloy. As a result, the $\alpha\text{-}Fe_6Ga_5$ and $\beta\text{-}Fe_6Ga_5$ ($Fe_{13}Ga_{13}$) phases are not detected in the surface layer after the heating-cooling cycle of Fe-45Ga alloy. The phase composition determined in this sample by ND is completely different from the XRD data from the surface: the $Fe_{13}Ga_{13}$ (85%), as well as B2 (6%) and $L1_2$ (9%) phases, are recorded in the bulk sample after the heating-cooling cycle. This means that heating with a constant rate of 2 °C/min up to 770 °C, holding at this temperature for 1.5 h and subsequent cooling do not lead to the appearance of the $\alpha\text{-}Fe_6Ga_5$ phase. Significantly longer annealing times are required to begin this phase transition.

CRediT author contribution statement

T.N. Vershinina: Formal analysis, structural calculations, text, Writing – original draft. **I.A. Bobrikov:** X-Ray and neutron diffraction experiment, Rietveld refinement. **S.V. Sumnikov:** X-Ray and neutron diffraction experiment. **A.O. Boev:** DFT calculations; A.M. Balagurov, Conceptualization, Formal analysis, Writing – original draft. **A.M. Balagurov:** Producing of alloy and samples, Investigation. **A.K. Mohamed:** Conceptualization, Writing – original draft.

Declaration of competing interest

The authors declare that they have no known competing financial interests or personal relationships that could have appeared to influence the work reported in this paper.

Acknowledgments

The neutron diffraction data were obtained using the IBR-2 (JINR) neutron source. The authors are grateful to V.G. Simkin for assistance with the neutron diffraction experiment. This work was financially supported by Russian Foundation for Basic Research (grant No. 18-58-52007). A.K.M. acknowledges the financial support of the Ministry of Education and Science of the Russian Federation in the framework of Increase Competitiveness Program of NUST MISiS.

References

[1] H. Okamoto, The Fe-Ga (Iron-Gallium) system, Bulletin of Alloy Phase Diagrams 11 (1990) 576–581, https://doi.org/10.1007/BF02841721.
[2] A.E. Clark, J.B. Restorff, M. Wun-Fogle, T.A. Lograsso, D.L. Schlagel, Magnetostrictive properties of body-centered cubic Fe-Ga and Fe-Ga-Al alloys, IEEE Trans. Magn. 36 (2000) 3238–3240, https://doi.org/10.1109/20.908752.
[3] A.E. Clark, K.B. Hathaway, M. Wun-Fogle, J.B. Restorff, T.A. Lograsso, V. M. Keppens, G. Petculescu, R.A. Taylor, Extraordinary magnetoelasticity and lattice softening in bcc Fe-Ga alloys, J. Appl. Phys. 93 (2003) 8621–8623, https://doi.org/10.1063/1.1540130.
[4] A.G. Khachaturyan, D. Viehland, Structurally heterogeneous model of extrinsic magnetostriction for Fe-Ga and similar magnetic alloys: Part I. Decomposition and confined displacive transformation. Part II. Giant Magnetostriction and Elastic Softening, Metallurgical and Materials Transactions A38 (2007) 2308–2316, https://doi.org/10.1007/s11661-007-9252-0. , 2317-2328.
[5] I.S. Golovin, V.V. Palacheva, A.K. Mokhamed, A.M. Balagurov, Structure and properties of Fe–Ga alloys as promising materials for electronics, Phys. Met. Metallogr. 121 (2020) 851–893, https://doi.org/10.1134/S0031918X20090057.
[6] A.K. Mohamed, V.V. Cheverikin, S.V. Medvedeva, I.A. Bobrikov, A.M. Balagurov, I. S. Golovin, First and second order phase transitions in Fe-(17-19)at.%Ga alloys, Mater. Lett. 279 (2020) 128508, https://doi.org/10.1016/j.matlet.2020.128508.
[7] A.K. Mohamed, V.V. Palacheva, V.V. Cheverikin, E.N. Zanaeva, W.C. Cheng, V. Kulitckii, S. Divinski, G. Wilde, I.S. Golovin, The Fe-Ga phase diagram: revisited, JALCOM 846 (2020), https://doi.org/10.1016/j.jallcom.2020.156486, 156486 (1-11).
[8] R.W.G. Wyckoff, Crystal Structures, John Wiley, New York, 1963.
[9] A.M. Balagurov, I.S. Golovin, I.A. Bobrikov, V.V. Palacheva, S.V. Sumnikov, V. B. Zlokazov, Comparative study of structural phase transitions in bulk and powdered Fe-27Ga alloy by real-time neutron thermodiffractometry, J. Appl. Crystallogr. 50 (2017) 198–210, https://doi.org/10.1107/S1600576716020045.
[10] I.S. Golovin, A.M. Balagurov, Structure Induced Anelasticity in Iron Intermetallic Compounds and Alloys, Materials Research Forum LLC, USA, 2018, p. 256.
[11] B. Malaman, M.J. Phillippe, B. Roques, A. Courtois, J. Protas, Structures cristallines des phases Fe_6Ge_5 et Fe_6Ga_5, Acta Crystallogr. B30 (1974) 2081–2087, https://doi.org/10.1107/S0567740874006522.

[12] K. Schubert, T.R. Anantharaman, H.O.I. Ata, H.G. Meissner, M. Pötzschke, W. Rossteutscher, E. Stolz, et al., Einige strukturelle ergebnisse an metallischen phasen (6), Die Naturwissenschaffen 47 (1960) 512, https://doi.org/10.1007/BF00600681.
[13] H.G. Meissner, K.Z. Schubert, Zum Aufbau einiger zu T^5-Ga homologer und quasihomologer Systeme, Z. Metallkd. 56 (1965) 523–530.
[14] O. Gourdon, S.L. Bud'ko, D. Williams, G.J. Miller, Crystallographic, electronic, and magnetic studies of ζ_2-GaM (M = Cr, Mn or Fe): Trends in Itinerant Magnetism, Inorganic Chemistry 43 (2004) 3210–3218, https://doi.org/10.1021/ic035419f.
[15] I.S. Golovin, A.M. Balagurov, I.A. Bobrikov, S.V. Sumnikov, A.K. Mohamed, Cooling rate as a tool of tailoring structure of Fe-(9-33%)Ga alloys, Intermetallics 114 (1–5) (2019) 106610, https://doi.org/10.1016/j.intermet.2019.106610.
[16] A. Leineweber, H. Becker, A.O. Boev, I.A. Bobrikov, A.M. Balagurov, I.S. Golovin, Fe13Ga9 Intermetallic in Bcc-Base Fe-Ga Alloy, Intermetallics 131 (2021) 107059, https://doi.org/10.1016/j.intermet.2020.107059.
[17] O. Kubaschewski, Iron-binary Phase Diagrams, Springer-Verlag Berlin Heidelberg GmbH, 1982.
[18] A.M. Balagurov, Scientific reviews: high-resolution fourier diffraction at the IBR-2 reactor, Neutron News 16 (2005) 8–12, https://doi.org/10.1080/10446830500454346.
[19] W. Kohn, L.J. Sham, Self-consistent equations including exchange and correlation effects, Phys. Rev. 140 (1965) A1133–A1138, https://doi.org/10.1103/physrev.140.a1133.
[20] G. Kresse, J. Furthmüller, Efficiency of ab-initio total energy calculations for metals and semiconductors using a plane-wave basis set, Comput. Mater. Sci. 6 (1996) 15–50, https://doi.org/10.1016/0927-0256(96)00008-0.
[21] D. Aksyonov, S. Fedotov, K. Stevenson, A. Zhugayevych, Understanding migration barriers for monovalent ion insertion in transition metal oxide and phosphate based cathode materials: a DFT study, Comput. Mater. Sci. 154 (2018) 449–458, https://doi.org/10.1016/j.commatsci.2018.07.057.
[22] J.P. Perdew, K. Burke, M. Ernzerhof, Generalized Gradient Approximation Made Simple, Physical Review Letters 77 (18) (1996) 3865–3868, https://doi.org/10.1103/physrevlett.77.3865.
[23] A. Jain, S.P. Ong, G. Hautier, W. Chen, W.D. Richards, S. Dacek, S. Cholia, D. Gunter, D. Skinner, G. Ceder, et al., Commentary: the Materials Project: a materials genome approach to accelerating materials innovation, Apl. Mater. 1 (1) (2013), https://doi.org/10.1063/1.4812323, 011002.
[24] G. Nolze, PowderCell: a mixture between crystal structure visualizer, simulation and refinement tool, Proc. II Int. School on Powder Diffraction (2002) 146–155.
[25] J. Rodrıguez-Carvajal, Recent advances in magnetic structure determination by neutron powder diffraction, Physica B 192 (1993) 55–69, https://doi.org/10.1016/0921-4526(93)90108-I.
[26] O. Gourdon, G.J. Miller, Reinvestigation of the GaMn structure and theoretical studies of its electronic and magnetic properties, J. Solid State Chem. 173 (1) (2003) 137–147, https://doi.org/10.1016/s0022-4596(02)00031-2.
[27] K. Lejaeghere, V. Van Speybroeck, G. Van Oost, S. Cottenier, Error estimates for solid-state density-functional theory predictions: an overview by means of the ground-state elemental crystals, Crit. Rev. Solid State Mater. Sci. 39 (1) (2014) 1–24, https://doi.org/10.1080/10408436.2013.772503.
[28] S. Paranthaman, Assessment of DFT functionals in predicting bond length and atomization energy of catalytically important metal dimers, Croat. Chem. Acta 90 (1) (2017) 17–26, https://doi.org/10.5562/cca2973.
[29] S. Geller, Crystal Structure of β-Ga_2O_3, The Journal of Chemical Physics 33 (3) (1960) 676–684, https://doi.org/10.1063/1.1731237.
[30] I.S. Golovin, A.M. Balagurov, I.A. Bobrikov, V.V. Palacheva, J. Cifre, Phase transition induced anelasticity in Fe-Ga alloys with 25 and 27%Ga, J. Alloys Compd. 675 (2016) 393–398, https://doi.org/10.1016/j.jallcom.2016.03.142.
[31] I.A. Bobrikov, N.Yu Samoylova, S.V. Sumnikov, O.Yu Ivanshina, K.A. Korneeva, A. M. Balagurov, I.S. Golovin, Temperature evolution of Fe-27Ga structure: comparison of in situ X-ray and neutron diffraction studies, J. Appl. Crystallogr. 53 (2020) 1343–1352, https://doi.org/10.1107/S1600576720010948.
[32] J.H. Hubbell, S.M. Seltzer, Tables of X-Ray Mass Attenuation Coefficients and Mass Energy Absorption Coefficients 1 keV to 20 MeV for Elements Z = 1 to 92 and 48 Additional Substances of Dosimetric Interest, NISTIR-5632, 1995.
[33] B. Alhalaili, R. Vidu, M.S. Islam, The growth of Ga_2O_3 nanowires on silicon for ultraviolet photodetector, Sensors 19 (2019) 5301, https://doi.org/10.3390/s19235301.
[34] Z. Nie, Z. Wang, Y. Liang, D. Cong, G. Li, C. Zhu, Y. Wang, Structural investigations of Fe-Ga alloys by high-energy x-ray diffraction, J. Alloys Compd. 763 (2018) 223–227, https://doi.org/10.1016/j.jallcom.2018.05.327.
[35] I.S. Golovin, A.M. Balagurov, V.V. Palacheva, I.A. Bobrikov, V.B. Zlokazov, In-situ neutron diffraction study of bulk phase transitions in Fe-27Ga alloys, Materials Design 98 (2016) 113–119, https://doi.org/10.1016/j.matdes.2016.03.016.
[36] A.M. Balagurov, I.A. Bobrikov, I.S. Golovin, Effects of ordering in Fe-xAl alloys, JETP Lett. (Engl. Transl.) 110 (2019) 585–591, https://doi.org/10.1134/S0021364019210057.
[37] S.-M. Na, A.B. Flatau, Magnetostriction and surface-energy-induced selective grain growth in rolled Galfenol doped with sulfur, Smart Structures and Materials 2005: Active Materials: Behavior and Mechanics (2005), https://doi.org/10.1117/12.599743.